NUMERICAL ANALYSIS OF PULSED NEUTRON GENERATION FROM 12 TW 50 fs LASER WITH DEUTERIUM CLUSTER

W. Ghaly[1], T. Masaki[2], Y. Kishimoto[2] and M. Uesaka[1]

[1]Nuclear Engineering Research Laboratory, University of Tokyo
22-2 Shirane- Shirakata, Tokai, Naka, Ibaraki, 319-1188, JAPAN.
[2]JAERI, Naka Fusion Research Establishment, Naka-machi, Naka-gun,
Ibaraki-ken, 311-0139, JAPAN

Abstract

It has been recognized that irradiation of intense laser on atomic cluster leads to a number of novel phenomena, including efficient heating of electron, rapid and efficient subsequent heating of ions, and efficient emission of X-ray. Recently, it has been shown that the high energy ions can yield fusion reaction and neutron generation. We present 2-dimensional Particle–In-Cell simulations of atomic cluster explosions by interaction with a high-intensity femtosecond laser pulse. We investigate the dynamics of deuterium cluster explosion providing information about time-resolved ion energy spectra for various laser intensities and cluster sizes. Our present simulation is done for single cluster-laser interaction.

1 INTRODUCTION

The interaction of laser pulses with atomic and molecular clusters has become a subject of great interest. Recent experiments show that the interaction of short (femtosecond), intense (>10^{16} W/cm^2) laser pulses with rare gas clusters is responsible for the generation of highly energetic electrons and ions [1,2], enhanced emission of X-rays in the keV range [3], Coulomb explosion of clusters [4,5], coherent high harmonic generation [6] and applications to nuclear fusion [7].

We present a novel approach to describe accurately the dynamics of laser-cluster interaction by using a Particle-in- Cell (PIC) code, determining the position, momentum and energy under influence of both external laser field and the fields generated by the particle themselves, for a very large number of particles and within a reasonable time. By using the 2-dimensonal PIC J-EM2D numerical code, we investigate fundamental physical processes of laser energy absorption by clusters, energy conversion to cluster electrons and ions, their energy distributions, expansion dynamics of clusters, fusion cross-section and neutron yield.

2 TWO-DIMENSIONAL PIC SIMULATION

2.1 Simulation set-up

2D simulations were done using the fully relativistic Particle-In-Cell code J-EM2D [8].

In a series of simulation, we employ the periodic boundary condition both in x- and y-directions with the size of L_x and L_y (and usually, $L_x = L_y$). Our simulation frame was 790 nm × 790 nm. We consider that 12 TW 50fs laser pulse travels and propagates in the x-direction, while the polarization of the laser electric field is in the y-direction. We handle 2-dimensinal circular rod-like clusters with radius a and constant ion density n_{cl}. In all cases, we chose the laser wavelength as $\lambda_l = L_x$ (= 820 nm) and treated one cluster located at $(x,y) = (L_x/2, L_y/2)$. Since the simulation box is periodic both in the x- and y-directions, the packing fraction is defined in the 2-dimensonal by $f \equiv n_{av}/n_{cl} = a^2/R^2 \equiv f_D$, where n_{av} the average ion density after laser-cluster interaction, n_{cl} the ion density before interaction, a the cluster radius, and R given by $R=(S/\pi N_{cl})^{1/2}$ and N_{cl} the number of cluster in the area ($S= L_x L_y$). We should note that the laser-cluster interaction and resultant expansion process are qualitatively different between 2- and 3-dimensional cases. Also the laser-cluster interaction is characterized using the relation among the cluster size a, the electron skin depth to cluster size ($\delta_e \equiv \omega_p/c$), ω_p the plasma frequency, and ξ_e the electron excursion length.

2.2 Simulation results

2.2.1 Large cluster size 32 nm ($\delta_e < a \sim \xi_e$)

Figure 1 shows the time evolution of the relative laser field, electron and ion energies. We define the conversion ratio from the initial laser energy to electron and ion energies by $\eta_i = E_i / E_l^{(0)}$, $\eta_e = E_e/E_l^{(0)}$ and the total conversion ratio $\eta_{abs} = (E_{i+} E_e)/E_l^{(0)}$ where E_e, E_i and $E_l^{(0)}$ the electron, ion and laser energy at t=0 respectively. In the early phase of interaction at $t \leq 21.4$ fs, the laser energy absorbed by clusters electrons then the ion energy gradually increases. At t=50 fs, the electron energy saturates, while the ion kinetic energy keeps increasing and surpasses the electron energy. Finally, the large fraction of the laser energy is transferred to deuterium ions $\eta_i \cong 55$ %. The total absorption gain η_{abs} becomes 67%. The electron energy gain slightly decreases after saturation from η_e~21% to 13%, suggesting that the electrons are cooled during the ion expansion.

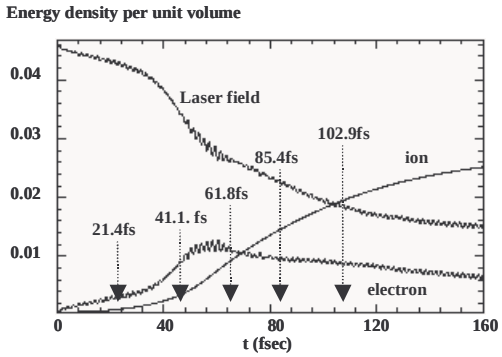

Fig.1 Time-evolution of laser field energy, electron and ion kinetic energies for the cluster size of 32 nm.

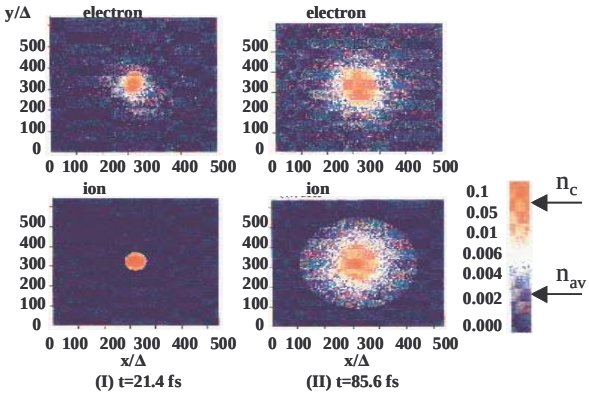

Fig.2 Electron and ion number density distributions at 21.4, 85.6 fs for cluster size of 32 nm.

Figure 2 shows the electron and ion number density distributions in the frame at the early interaction time (21.4fs) and the later time (85.4fs). The clear high-density electron core exists, many clusters electrons leave the host cluster and distribute over the entire frame. From Figs. 1 and 2, the process of ion energy gain can be regarded the *ambipolar* expansion due to the electrostatic acceleration near the ion front. The electrostatic field that arises from the local charge separation near the ion vacuum interface accelerates ions to higher energies. The *ambipolar* expansion is triggered by strong electrostatic field due to the electron pressure induced in the ion expansion front. *ambipolar* expansion due to the electrostatic acceleration near the ion front. The electrostatic field that arises from the local charge separation near the ion vacuum interface And the plasma expand into vacuum and subsequent fast ions are generated as shown in Fig. 4.

Figure 3 shows the electron and ion energy distributions at different times. The cluster electrons are rapidly heated in the early interaction phase. At t=21.4fs a high-energy tail component with two temperatures is formed. At t=42.7 fs the distribution function is fully developed and after this time the high-energy component gradually reduces. This results from the cooling of electrons served n Fig. 1. At t=107.2 fs the average electron energy is 12 keV, but the tail component is approximately 20 keV. Fig. 3(b), the ions are slowly accelerated in accordance with he development of the electron energy distribution and shown a nearly flat component of high energies with a sharp edge and the average ion energy reaches 46 keV with high-energy ions beyond 100 keV in the last distribution. Such nearly flat energy distribution may be effective in producing large amount of DD-fusion reactions, since the cross section greatly increases as deuterons exceed 100 keV. By employing obtained ion distributions as shown in Fig. 3, we estimate the fusion yield assuming the interaction region by the plasma filament with the diameter 100 μm and axial length 500 μm (interaction volume: 3.39×10^{-6}cm^{-3}) and the disassembly time τ_d of 20 ps. The estimated fusion cross section is $\langle\sigma v\rangle_{DD}\cong1.74\text{X}10^{-17}$cm^{3}sec^{-1} and the total reaction rate is $\langle\sigma v\rangle_{DD}n_D^2 \cong 8.32\text{X}10^{23}$ cm^{-3}sec^{-1}. The expected fusion neutron yield is estimated as $N\cong3.2\times10^7$ by using the equation $N\cong(\tau_d/2)\int\langle\sigma v\rangle_{DD}\, n_D^2\, dV$.

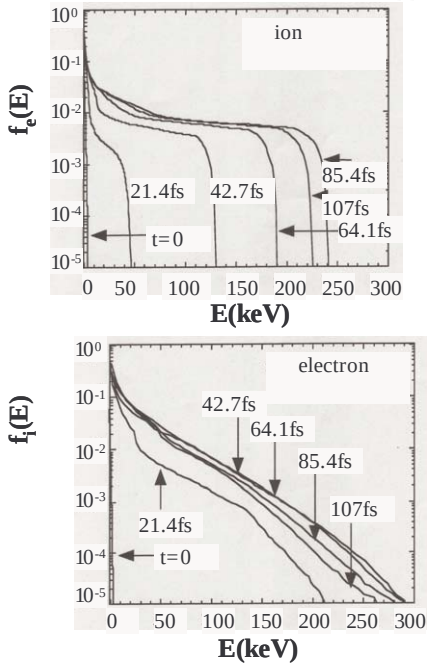

Fig. 3 Electron and ion energy distributions at different times for cluster radius a=32 nm and high density

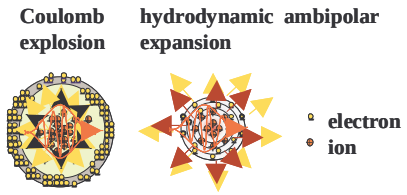

Fig. 4 Coulomb explosion and hydrodynamic ambipolar expansion

2.2.2 Small cluster size 16 nm ($a<\delta_e<\xi_e$)

As the cluster size becomes small ($a\sim$ 16 nm), the total particle number and corresponding Coulomb energy contained per cluster become small. The laser energy conversion is also relatively small compared with the case of a=32 nm. This is because the number of electrons interacting with the laser field N_{int} is smaller in the case of

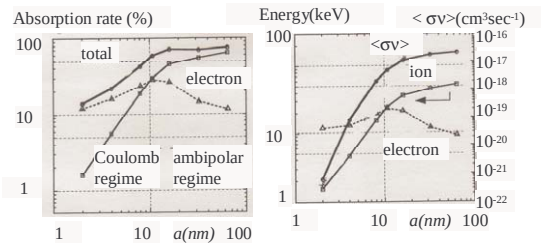

Fig. 5 Absorption rate of laser filed, electron and ion energies and fusion yield vs. cluster size for high density $2.19\times10^{20}cm^{-3}$

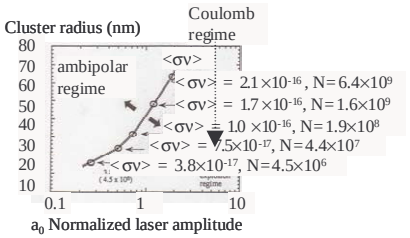

Fig. 6 Cluster size vs. normalized laser amplitudes

a =16 nm than in the case of a=32 nm. By analysing the electron and ion density energy distributions for the small cluster size, it is concluded that the expansion process belongs to the *Coulomb* explosion. When all the clusters electrons expelled from the original cluster core during a few laser optical cycles and the cluster becomes highly positively charge so the Coulomb energy chemically stored inside the cluster and this process known as *Coulomb* explosion. See Fig. 4.

2.2.3 High-density case

Total absorption rate η_{abs} increase with the cluster size in the small cluster regime (2nm≤a≤10nm). At a≤7 nm (i.e. the small cluster regime), the conversion to electron energy η_e is dominant, while the conversion to ion energy rapidly increases according to $\eta_i^{0.8}$. At 7<a<16 nm, a significant amount of the absorbed energy is transferred to ions and the conversion to electron energy decreases, as shown in Fig. 5. At a > 16 nm, the ion kinetic energy tends to saturate at a much lower level. This result is understood as follows. When the cluster size is small like $a < \delta_e$(~25 nm), the laser field fully penetrates the entire cluster and the number of interacting electrons is proportional to a^2. As the cluster size increases, the laser field exponentially attenuates toward the centre, and the effective number of interacting electrons decreases. As the cluster size further increases, the laser field only interact with the peripheral region and the number of interacting electrons is proportional to a. The fusion yield increases as the cluster size increases. At a > 16 nm, the ion kinetic energy tends to saturate and the neutron yield also become saturates.

2.2.4 Laser amplitude and cluster size effect

Figure 6 shows the critical line on the plane of cluster radius a and normalized laser amplitude a_o ($a_o=8.6\times10^{-10}\lambda[\mu m]\ I^{1/2}[W/cm^2]$, and $I= 2P/\pi r_o$, where λ the laser wavelength, P the laser power and r_o the laser focusing spot size). If we focus 12 TW 50 fs laser with spot size 10 μm, we have $I = 7.6\times10^{18}\ W/cm^2$ and a_o =1.9. This critical line shows the boundary between the ambipolar expansion regime and the Coulomb explosion regime. The fusion cross section increases for larger cluster size. By increasing the cluster size, we need to increase the laser amplitude to obtain a higher neutron yield. If we use the cluster of 50 nm radius for a_o =1.9, we estimate the number of neutrons per shot ~ 1.6×10^9.

3 CONCLUSION

We have investigated the single laser-cluster interaction numerically in the 2-dimensional configuration to understand the dynamics of energetic electrons, ions and nuclear fusion reaction. The expansion of laser-irradiated clusters is characterized by the relation among the cluster size a, the electron skin depth δ_e and the electron excursion length ξ_e. Depending on those parameters, the expansion is categorized into the hydrodynamic ambipolar explosion and the Coulomb explosion. The ambipolar expansion takes place in larger cluster case $a >> \delta_e \sim \xi_e$, whereas the Coulomb explosion in the smaller cluster size $a << \delta_e \sim \xi_e$.

We calculated the electron and ion energy distributions, and the fusion reaction rate for various cluster sizes, cluster densities and laser amplitudes. Although the analysis is limited to the simple single cluster-laser interaction in 2-deminsonal configuration, we have shown the possibility to generate ~ 1.6×10^9 neutrons by using the 12TW 50fs laser and the cluster of 50 nm radius. We plan to consider more realistic configuration than the 2-dimensional case and carry out the experiment.

REFERENCES

[1] Y. L. Shao et al, *Phys Rev. Lett* . **77**, 3343 (1996).
[2] T. Ditmire et al, *Nature.* **368**, 54, (1996).
[3] S. Dobosz et al, *Phys. Rev. A.* **56**, R2526, (1997).
[4] N. G. Gotts et al, *J. Chem. Phys.* **96**, (1962).
[5] J. Purnell et al, *Chem. Phys. Lett.* **229**, 33e (1994).
[6] T. D. Donnelly et al, *Phys. Rev. Lett.* **76**,2472 (1996).
[7] T. Ditmire et al, *Nature.* **398**, 489, (1999).
[8] Y. Kishimoto (private communication): 2-dimensional fully relativistic electromagnetic particle in cell code , J-EM2D, Japan Atomic Energy Research Institute, Naka, Dept. of Physics (2001).